The Mechanism of Pressure-Driven Band Gap Evolutions in Lead-Free Halide Double Perovskites

Lingjun He[a], Yuanhui Sun[b,], Maosheng Miao[b], and Haiqing Lin[a,*]*

[a]*Simulations of Physical Systems Division, Beijing Computational Science Research Center, Beijing 100193, China*
[b]*Department of Chemistry and Biochemistry, California State University Northridge, Northridge, CA 91330, USA*

ABSTRACT: Lead-free halide double perovskites Cs_2BBiCl_6 (B = Na, Ag) are potential alternatives in optoelectronic application because of their nontoxicity and intrinsic stability. Intriguingly, the photoluminescence spectra of their cubic phases revealed that the band gap evolution under pressure strongly depends on B−site metals. Our first-principles calculations demonstrate that this distinct phenomenon is caused by orbital contributions of B−site cations (Na versus Ag) at the band edges. In contrast to Na in $Cs_2NaBiCl_6$ whose 3*s* valence orbitals contribute insignificantly to the band edge states, Ag in $Cs_2AgBiCl_6$ can cause large upward shifts of the valence band maximum energy under pressure because of the enlargement of bonding-antibonding energy split of Ag−Cl bonds below the Fermi level. Other double perovskites with different B−site cations (K, Rb, Cu, and Au) in +1 valence state exhibit similar band gap evolutions as $Cs_2NaBiCl_6$ and $Cs_2AgBiCl_6$, respectively, indicating that B−site cation play a critical role in regulating the electronic properties of lead-free halide double perovskites. Moreover, our calculations show that the optical absorbance coefficients of $Cs_2CuBiCl_6$ and $Cs_2AuBiCl_6$ can be as large as 10^5 cm^{-1} in the region of visible lights, and could be further enhanced by external pressure. Our study reveals the mechanism of how *s/d*-block metals regulate the band gap of double perovskites, and provides a guideline for the band engineering of optoelectronics under high pressure.

TOC Graphic

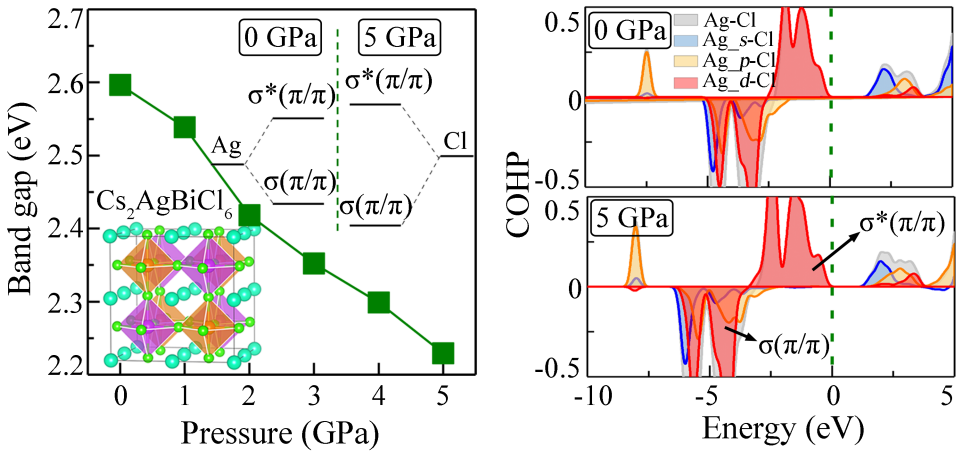

INTRODUCTION

The lead halide perovskites with a chemical formula of $APbX_3$ (A = Cs^+, $CH_3NH_3^+$, $CH(NH_2)_2^+$; X = Cl^-, Br^-, I^-) have attracted considerable attentions due to their excellent properties including strong light absorption, long carrier diffusion length, high carrier mobility, and tunable band gaps.[1–4] However, their commercialization is primarily restricted by their instability and the toxicity of Pb.[5,6] Pb-free halide double perovskites $A_2B^+B^{3+}X_6$, which could be formulated through the substitutions of two Pb^{2+} in the crystal lattice with a pair of nontoxic monovalent B^+ (e. g., Na^+, Ag^+, In^+) and trivalent B^{3+} (e. g. Sb^{3+}, Bi^{3+}, In^{3+}) metal cations, are promising $APbX_3$ replacements with no toxicity and enhanced stability.[7–12] These Pb-free halide perovskites also exhibit great potential for applications in photodetectors, X-ray detectors, photocatalysts, light-emitting diodes (LED), *etc*.[13–16]

Despite of the enormous attention and progresses in recent years, these materials exhibit wide bandgaps and low luminescence, which severely restrict their applications in optoelectronic field.[17–19] To solve this problem, many efforts are committed, including compositional variation,[12,20,21] chemical substitution,[22,23] and high-pressure technique.[24–27] Especially, high-pressure is a powerful tool that can effectively modify the structural and electronic properties of materials without chemically changing the materials.[28] By applying pressure, recent studies successfully reduced the band gap of $Cs_2AgBiBr_6$ from ~2.2 eV to 1.7 eV[27] and regulated photoluminescence emission range in $Cs_2AgBiCl_6$ and $Cs_2NaBiCl_6$.[29,30] Interestingly, the band gap of $Cs_2NaBiCl_6$ increases with pressure up to ~5 GPa, whereas the band gaps of $Cs_2AgBiCl_6$/$Cs_2AgBiBr_6$ decrease with pressure in the studied range (< 5 GPa for $Cs_2AgBiCl_6$ or < 3 GPa for $Cs_2AgBiBr_6$). Then they will transform to a tetrahedral structure at higher pressure. The researchers have explained the phenomena of individual structures, but no discussion on the overall understanding was reported. The main difference between the two sets of perovskites is the B−site cations, namely Na is an *s*-block element and Ag is a *d*-block element. Would the above bandgap trend be general for halide double perovskites with other *s/d*-block metals (K, Rb, Cu, and Au) in +1 valence state? In order to answer this question, we first need an in-depth understanding of the intricate band gap evolution under pressure.

In this work, we perform density functional theory (DFT) calculations to thoroughly investigate the band gap evolutions of cubic $Cs_2NaBiCl_6$ and cubic $Cs_2AgBiCl_6$ under increasing pressure (< 5GPa). Our results agree with the experimental observations and demonstrate the importance of different B−site cations in modulating the electronic structures of double perovskites. By calculating the calculated orbital projected band structures and bond analyses, we show that the conduction band minimums (CBMs) of $Cs_2NaBiCl_6$ goes up slightly more than valence band maximums (VBMs), due to the stronger response of Na−3*s* orbitals to pressure. In contrast, the VBMs of $Cs_2AgBiCl_6$ mainly consisting of Ag−4*d* and Cl−3*p* orbitals result in an upward shift of ~3.1 times with respect to CBMs while the pressure increases from 1 atm to 5 GPa. Our calculations also show that similar perovskites with other B−site elements in +1 valence state exhibit the same bandgap evolution trend under increasing pressure. To evaluate their sunlight harvest performance for potential photovoltaic or optoelectronic applications, their optical absorbance spectra are also calculated here. Especially, $Cs_2CuBiCl_6$ and $Cs_2AuBiCl_6$ show tunable band gap evolutions of 1.59−1.76 eV and 1.08−1.36 eV in the pressure range of 1 atm to 5 GPa, respectively, which indicates excellent optical absorbance in the visible region of light.

COMPUTATIONAL DETAILS

All the first-principles DFT calculations were performed based on plane-wave pseudopotential method as implemented in Vienna Ab initio simulation package (VASP).[31,32] The electron-ion interactions were described by the projected augmented wave pseudopotential (PAW).[33,34] A plane-wave energy cutoff of 500 eV was used to ensure good convergence of the total energy with an energy precision of 10^{-7} eV. The atomic positions were completely relaxed until the force acting on each atom is $<10^{-3}$ eV/Å. The Perdew−Burke−Ernzerhof (PBE)[35] functional was used for the structure optimizations, the Heyd−Scuseria−Ernzerhof (HSE) hybrid functional[36,37] was employed to evaluate the electronic structures, and GW with the Bethe−Salpeter equation (GW+BSE) method[38,39] was proposed for the analysis of optical properties. Spin-orbit coupling (SOC) is included in the electronic structure calculations. Crystal orbital Hamilton population (COHP) analysis as implemented in the LOBSTER package were also carried out to obtain information on the interatomic interactions.[40,41]

RESULTS AND DISCUSSION

Our calculations follow the approach of designing Pb-free double perovskites ($A_2B^+B^{3+}X_6$) by replacing two Pb^{2+} in two units of $APbX_3$ with a pair of monovalent and trivalent metal cations. For example, the two Pb^{2+} was replaced into [Na^+ + Bi^{3+}] and [Ag^+ + Bi^{3+}], generating two cubic double perovskites $Cs_2NaBiCl_6$ and $Cs_2AgBiCl_6$ (Figure 1).[42,43]

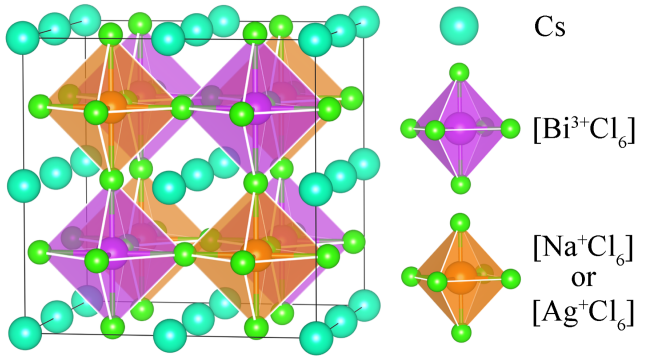

Figure 1. Crystal structure of double perovskite. The cesium atoms, $[Bi^{3+}Cl_6]$ and $[Na^{+}Cl_6]$/$[Ag^{+}Cl_6]$ octahedra are colored spring green, magenta, and orange, respectively.

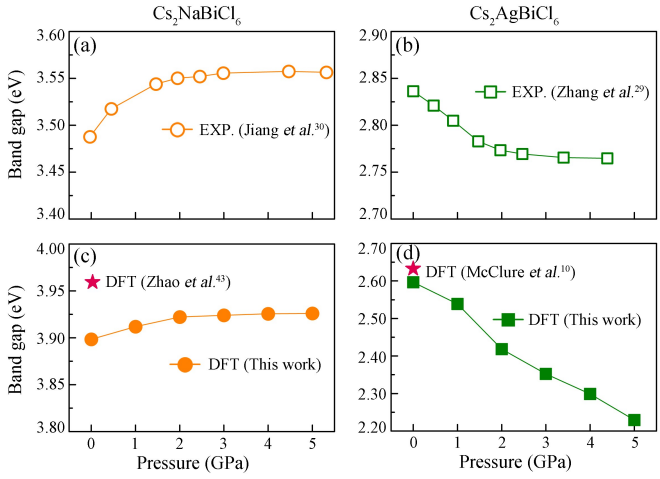

Figure 2. Band gap evolutions of (a) cubic $Cs_2NaBiCl_6$ and (b) cubic $Cs_2AgBiCl_6$ as a function of pressure in their photoluminescence spectra. Band gap evolutions of (c) cubic $Cs_2NaBiCl_6$ and (d) cubic $Cs_2AgBiCl_6$ as a function of pressure at the HSE06 hybrid functional level of theory. SOC effect is included in the calculations.

Firstly, the DFT calculations confirm the intricate band gap evolutions of cubic $Cs_2NaBiCl_6$ and cubic $Cs_2AgBiCl_6$ observed in photoluminescence spectra under pressure[29,30] (Figure 2). As shown in Figure 2c and 2d, the DFT band gap of $Cs_2NaBiCl_6$ gradually increases for 0.03 eV while pressure changes from 1 atm to 5 GPa, whereas the band gap of $Cs_2AgBiCl_6$ decreases for as large as 0.37 eV in the same pressure range. We note that our calculations overestimate the band gap changes with respect to the experiments (~0.08 eV). Previous DFT band gaps of $Cs_2NaBiCl_6$ and $Cs_2AgBiCl_6$ at 0 GPa are comparable to our calculations.[10,43] The change of the band gaps can be split into the changes of the band edge states (Figure 3). The CBMs and VBMs in Figure 3 are aligned with respect to the corresponding Cs−5*s* core level at a given pressure and we assume the average electrostatic potential of the whole unit cell does not significantly change while applying pressure up to 5 GPa. The results show both CBMs and VBMs go up with increasing pressure, and it is due to the different rate of changes between CBM and VBM that the band gaps of the double perovskites show different and intricate trends. For $Cs_2NaBiCl_6$, the CBM energy goes up slightly more than that of VBM. In contrast, the VBM energy of $Cs_2AgBiCl_6$ shifts upwardly for ~3.1 times of the change of CBMs while pressure increases from 1 atm to 5 GPa, resulting in a net band gap reduction of 0.37 eV.

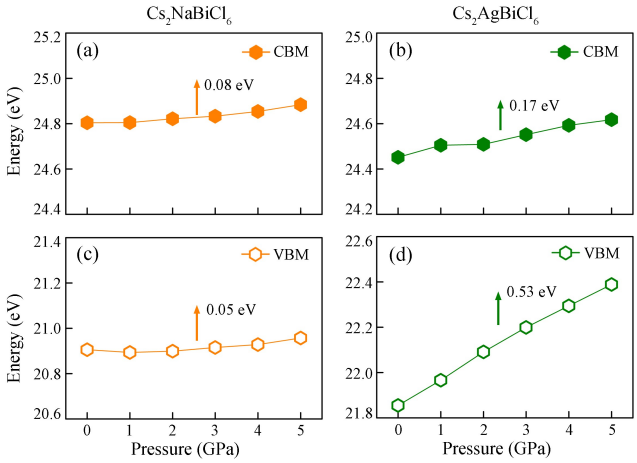

Figure 3. Evolutions of CBMs and VBMs of (a-b) $Cs_2NaBiCl_6$ and (c-d) $Cs_2AgBiCl_6$ as a function of pressure, respectively.

We carried out in-depth electronic structure analysis to find out what causes the above difference in bandgap changes of $Cs_2NaBiCl_6$ and $Cs_2AgBiCl_6$. Figure 4a and 4b depicted the atomic projected electronic band structures of cubic $Cs_2NaBiCl_6$ and $Cs_2AgBiCl_6$ at 5 GPa are calculated at the HSE06 hybrid functional level of theory. The corresponding band structures at 1 atm are shown in Figure S1. Both double perovskites show indirect bandgaps. For $Cs_2NaBiCl_6$, the CBM states are mainly composed of Bi−6*p* orbitals together with a small contribution of Na−3*s* orbitals, whereas the VBM mainly originates from Bi−6*s* and Cl−3*p* orbitals. For $Cs_2AgBiCl_6$, its CBM and VBM are dominated by extensive mixture of Ag−4*d*/Bi−6*p* and Cl−3*p* orbitals. These results agree with previous reports of double perovskite under 1 atm.[10,43] Under pressure, the orbital contributions to CBM and VBM states change slightly, indicating that the inverse band gap evolutions come from the different responses of these orbitals to increasing pressure. The orbitals of Bi atoms rarely affect the band gap evolutions in both $Cs_2NaBiCl_6$ and $Cs_2AgBiCl_6$, as discussed further below. The band states projected to Na atoms in $Cs_2NaBiCl_6$ and Ag atoms in $Cs_2AgBiCl_6$ (Figure 4c and 4d), show that Na−3*s* orbitals make small contributions to CBM states in $Cs_2NaBiCl_6$, whereas Ag−4*d* orbitals contribute significantly to both CBM and VBM of $Cs_2AgBiCl_6$.

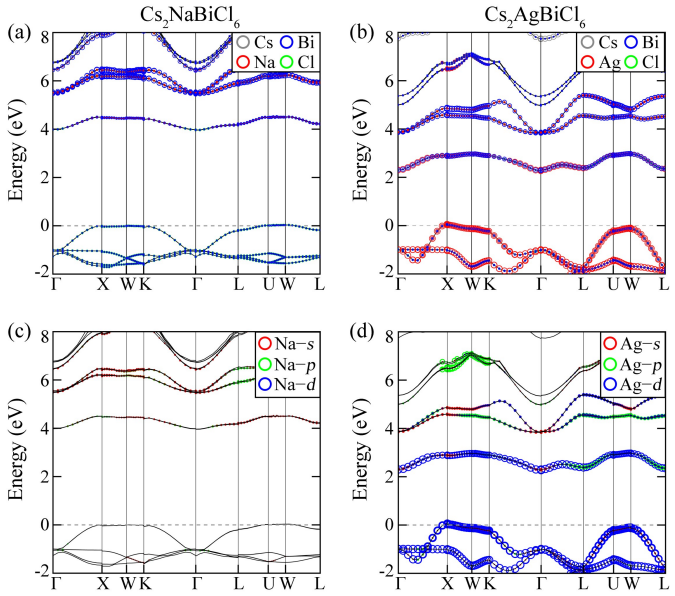

Figure 4. Atomic projected band structures of (a) $Cs_2NaBiCl_6$ and (b) $Cs_2AgBiCl_6$ at 5 GPa, respectively. Circles with different size represent the weight of orbital projection from each element (with gray for Cs, red for Na/Ag, blue for Bi, and green for Cl). Orbital projected band structures of Na and Ag atoms in (c) $Cs_2NaBiCl_6$ and (d) $Cs_2AgBiCl_6$ at 5 GPa, respectively. Circles with different size represent the weight of corresponding *s*/*p*/*d* orbital projection. (with red for *s* orbital, green for *p* orbital, and blue for *d* orbital).

COHP can show the feature and strength of chemical bonds. Negative COHP corresponds to bonding states, whereas positive COHP represents antibonding states. Moreover, the integrated COHP (ICOHP) up to the Fermi level can be used to measure the bong strength. While Na–Cl bond is mainly ionic and shows no important features in COHP, the bond between Ag–4*d* and Cl–3*p* are strongly covalent as revealed by corresponding COHP (Figure 5a). The first important feature that revealed by COHP is that the valence states close to Fermi level are antibonding states σ*(π/π) between π(Ag–4*d*) and π(Cl–3*p*) orbitals. However, Ag–Cl still form quite strong covalent bonds as its ICOHP values is about -1.95 eV/pair at Fermi level, although this value is much higher at a lower energy, for example -2.59 eV/pair at energy of -2.3 eV below Fermi level, while the antibonding-state COHP has not been integrated. More importantly, COHP calculations show that pressure has significant effects to Ag–Cl bonds. Besides improving the bond strength (Figure S2), it greatly broadens the bonding and antibonding bands because of the larger bonding-antibonding split under compression (Figure 5b). We note that the pressure-induced band dispersion is not responsible for this larger bonding-antibonding split. Therefore, COHP calculations distinctly show that the increase of the VBM energy under pressure in $Cs_2AgBiCl_6$ is caused by the enlargement of the bonding-antibonding energy split of Ag–Cl bonds.

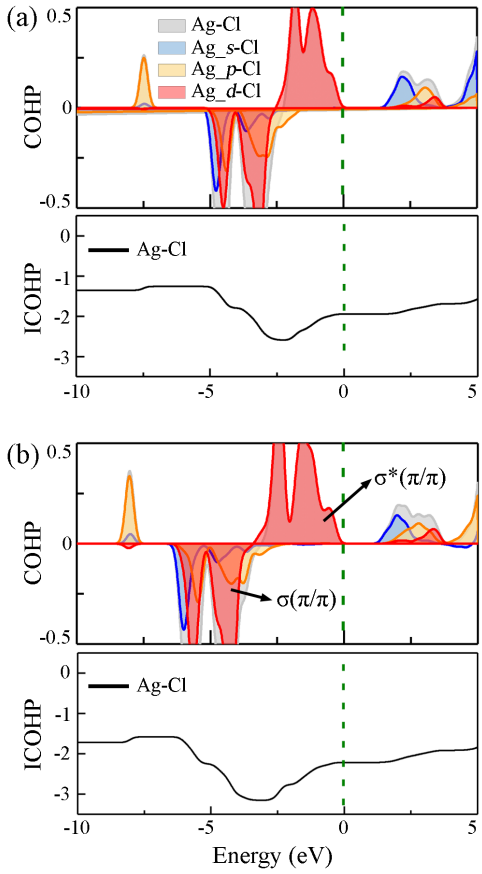

Figure 5. Calculated COHP and ICOHP of Ag–Cl bond in $Cs_2AgBiCl_6$ at (a) 1 atm and (b) 5 GPa, respectively.

To further validate the importance of B–site cations to the electronic properties of Pb-free halide double perovskites, we created a model compound by substituting Na or Ag metals in the double perovskites by noble gas Neon (Ne) and add 1 extra electron per Ne to maintain the electron counting. The calculations of the electronic structures of these model compounds reveal interesting insights. $Cs_2NaBiCl_6$ exhibits an almost identical band gap and a very similar pressure dependence as that of $[Cs_2NeBiCl_6]^-$ (Figure S3a). In contrast, replacing Ne by Ag metals reduces the band gap values from ~3.95 eV down to 2.23 eV and creates a strong pressure dependence (Figure S3b). The inert behavior of bandgap in $[Cs_2NeBiCl_6]^-$ demonstrate that the orbital contributions from Bi and Cl atoms in $Cs_2NaBiCl_6$ and $Cs_2AgBiCl_6$ are not sensitive to external pressure, rarely affect the band gap evolutions. The comparison of the atomic projected electronic band structures of $Cs_2AgBiCl_6$ and $[Cs_2NeBiCl_6]^-$ at 5 GPa (Figure S4) reveals distinct Ag–4*d* bands appearing in the gap of $[Cs_2NeBiCl_6]^-$, which further demonstrates the importance of Ag atom in the band gap engineering of $Cs_2AgBiCl_6$. The interaction in Ag–Cl bond raises the energy levels of antibonding σ*(π/π) states, and make them dominate the VBM states. Hence the opposite band gap evolutions in $Cs_2NaBiCl_6$ and $Cs_2AgBiCl_6$ should be ascribed to the distinct orbital features of B–site cations (Na and Ag atoms).

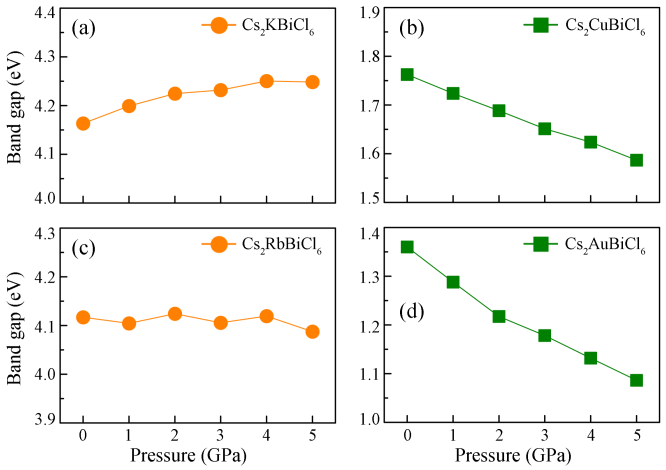

Figure 6. Evolutions of CBMs and VBMs of (a) $Cs_2NaBiCl_6$, (b) $Cs_2AgBiCl_6$, (c) $Cs_2CuBiCl_6$, and (d) $Cs_2AuBiCl_6$ as a function of pressure.

Furthermore, we like to examine whether the above opposite band gap trends of Na and Ag double perovskites can be extended to other *s*/*d*-block metals with +1 valence state. We calculate the band gap evolutions of double perovskites formulated by replacing Na (Ag) with K (Cu) or Rb (Au). As shown in Figure 6, the band gap of Cs_2KBiCl_6 increases for ~0.08 eV with pressure up to 5 GPa, and the gap of $Cs_2RbBiCl_6$ shows a small and nonmonotonic variation near 4.12 eV. For *d*-block perovskites, $Cs_2CuBiCl_6$ and $Cs_2AuBiCl_6$ show band gap reductions of ~0.17 eV and ~0.28 eV in the pressure range from 1 atm to 5 GPa, respectively. The corresponding atomic projected band structures at 5 GPa are shown in Figure S5. The evolutions of their CBMs and VBMs with varying pressure show similar trends but with different magnitudes as those in $Cs_2NaBiCl_6$ and $Cs_2AgBiCl_6$, respectively (Figure S6). Although the net variations of band gap for *s*-block perovskites are small, their CBM sand VBMs exhibit greater upward shifts when substitute Na to K or Rb metals, which are supposed to come from the heavier weight of K/Rb−*s*/*d* orbitals near CBMs or VBMs (Figure 7). It is worth mentioning that Cs_2KBiCl_6 and $Cs_2RbBiCl_6$ are direct band gap compounds in the pressure range from 1 atm to 5 GPa. The band edges in *d*-block perovskites (Cu, Ag and Au) show large monotonic increases with pressure and the shifts become more significant with increasing atomic number (Cu < Ag < Au). The strong antibonding state between Cu−3*d*/Au−5*d* orbitals and Cl atoms is also observed within the COHP analyses (Figure S7).

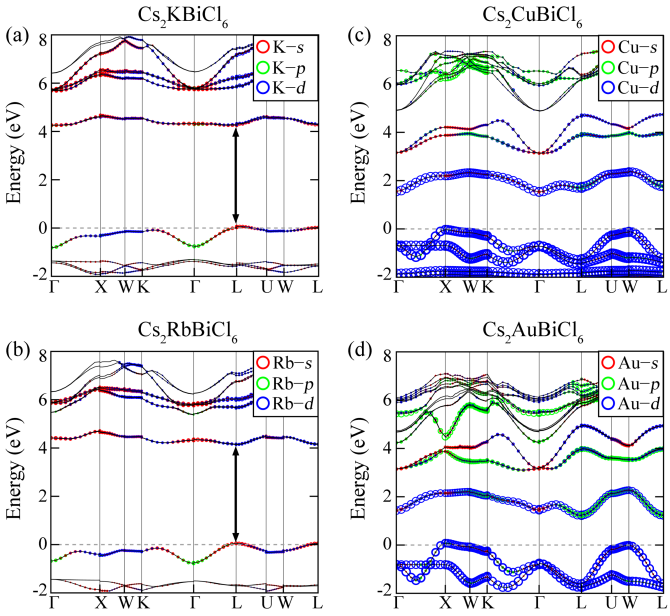

Figure 7. Orbital projected band structures of (a) K atom in Cs_2KBiCl_6, (b) Rb atom in $Cs_2RbBiCl_6$, (c) Cu atom in $Cs_2CuBiCl_6$, (d) Au atom in $Cs_2AuBiCl_6$ at 5 GPa, respectively. Circles with different size represent the weight of corresponding *s*/*p*/*d* orbital projection. (with red for *s* orbital, green for *p* orbital, and blue for *d* orbital).

The light absorption efficiency especially in the visible and ultraviolet regions is an essential property for photovoltaic conversion materials. To evaluate the sunlight harvest performance of above-mentioned Pb-free halide double perovskites, we calculated their optical absorbance spectra by employing the GW+BSE method, including self-energy and excitonic electron-hole interaction. As shown in Figure 8, the optical absorbance coefficients of the studied double perovskites Cs_2BBiCl_6 (B = Na, K, Rb, Cu, Ag, Au) may reach as high as 10^5 cm^{-1} in certain frequency range. In particular, the *d*-block double perovskites Cs_2BBiCl_6 (B = Cu, Ag, and Au) show large absorbance coefficients of about 10^5 cm^{-1} in the frequency region of visible lights. In contrast to alkali metal perovskites whose absorbance coefficients are insensitive to pressure, pressure more significantly broaden the absorption region of *d*-block perovskites especially $Cs_2CuBiCl_6$ and $Cs_2AgBiCl_6$, indicating an enhancement to their photovoltaic performance.

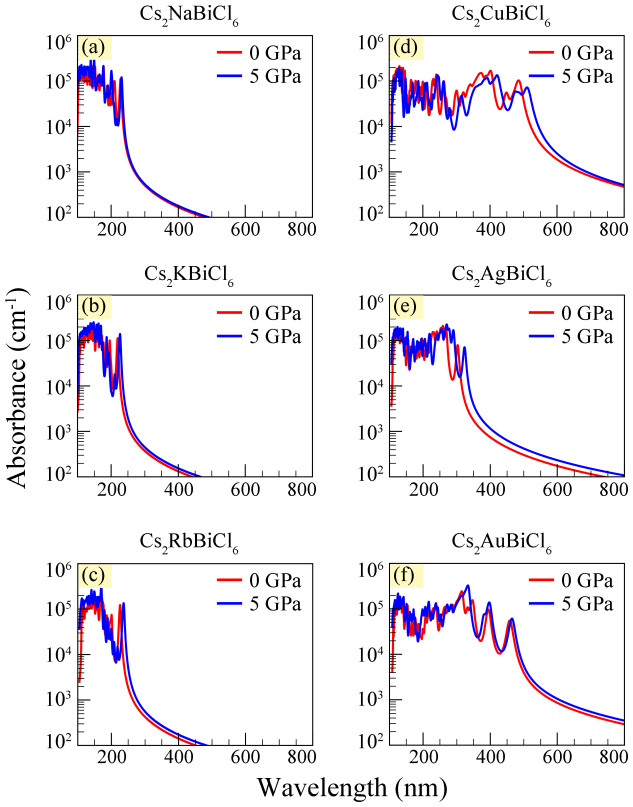

Figure 8. Optical absorbance of (a-c) *s*-block perovskites Cs_2MBiCl_6 (M = Na, K, Rb) and (d-f) *d*-block perovskites Cs_2MBiCl_6 (M = Cu, Ag, Au) at 0 and 5 GPa calculated by using the GW+BSE method.

CONCLUSIONS

In this work, we demonstrate the mechanism for the experimentally observed pressure-dependent band gap evolutions of $Cs_2NaBiCl_6$ and $Cs_2AgBiCl_6$ using first-principles DFT calculations. The insignificant contributions of Na orbitals at the CBMs of $Cs_2NaBiCl_6$ show little effect to band edge energies, and the band gap evolution is dominated by the chemical interactions between Bi and Cl atoms. In contrast, the VBMs of $Cs_2AgBiCl_6$ consist of the antibonding state between Ag−4*d* orbitals and Cl−3*p* orbitals, causing a large upward shift of VBM energy that is 3.1 times as the shift of CBM energy under 5 GPa. The bond analyses between B−site metals and neighboring Cl atoms and the Ne substitutions of B−site cations verify the important role of B−site cations in band engineering of double perovskites. Other *s/d*-block double perovskites show similar band gap evolutions and due to the same mechanism. Furthermore, our calculations show that the optical absorbance coefficients of $Cs_2CuBiCl_6$ and $Cs_2AuBiCl_6$ might become as high as 10^5 cm^{-1} in the region of visible light and could be further enhanced by external pressure.

ASSOCIATED CONTENT

Supporting Information

The Supporting Information is available free of charge at https://pubs.acs.org. The atomic and orbital projected band structures, evolutions of band gap and band edges, and ICOHP of studied Pb-free halide double perovskites under high pressure.

AUTHOR INFORMATION

*Corresponding Authors

*E-mail: yuanhui.sun@csun.edu
*E-mail: haiqing0@csrc.ac.cn

ORCID

Lingjun He: 0000-0003-4918-2792
Yuanhui Sun: 0000-0003-2981-1133
Maosheng Miao: 0000-0001-9486-1204

Notes

The authors declare no competing financial interest.

ACKNOWLEDGMENTS

L.H. is supported by the China Postdoctoral Science Foundation under grants No. 2021M690326. Y.S. and M.M. acknowledge the support of NSF under grant No. DMR-1848141. H.L. acknowledges financial support from NSAF U1930402 and computational resources from the Beijing Computational Science Research Center.

REFERENCES

(1) Eperon, G. E.; Leijtens, T.; Bush, K. A.; Prasanna, R.; Green, T.; Wang, J. T.-W.; McMeekin, D. P.; Volonakis, G.; Milot, R. L.; May, R.; et al. Perovskite-Perovskite Tandem Photovoltaics with Optimized Band Gaps. *Science* **2016**, *354* (6314), 861–865.

(2) Jeon, N. J.; Noh, J. H.; Yang, W. S.; Kim, Y. C.; Ryu, S.; Seo, J.; Seok, S. I. Compositional Engineering of Perovskite Materials for High-Performance Solar Cells. *Nature* **2015**, *517* (7535), 476–480.

(3) Protesescu, L.; Yakunin, S.; Bodnarchuk, M. I.; Krieg, F.; Caputo, R.; Hendon, C. H.; Yang, R. X.; Walsh, A.; Kovalenko, M. V. Nanocrystals of Cesium Lead Halide Perovskites ($CsPbX_3$, X = Cl, Br, and I): Novel Optoelectronic Materials Showing Bright Emission with Wide Color Gamut. *Nano Lett.* **2015**, *15* (6), 3692–3696.

(4) Sahli, F.; Werner, J.; Kamino, B. A.; Bräuninger, M.; Monnard, R.; Paviet-Salomon, B.; Barraud, L.; Ding, L.; Diaz Leon, J. J.; Sacchetto, D.; et al. Fully Textured Monolithic Perovskite/Silicon Tandem Solar Cells with 25.2% Power Conversion Efficiency. *Nature Mater.* **2018**, *17* (9), 820–826.

(5) Correa-Baena, J.-P.; Saliba, M.; Buonassisi, T.; Grätzel, M.; Abate, A.; Tress, W.; Hagfeldt, A. Promises and Challenges of Perovskite Solar Cells. *Science* **2017**, *358* (6364), 739–744.

(6) Rong, Y.; Hu, Y.; Mei, A.; Tan, H.; Saidaminov, M. I.; Seok, S. I.; McGehee, M. D.; Sargent, E. H.; Han, H.

Challenges for Commercializing Perovskite Solar Cells. *Science* **2018**, *361* (6408), eaat8235.

(7) Yang, B.; Mao, X.; Hong, F.; Meng, W.; Tang, Y.; Xia, X.; Yang, S.; Deng, W.; Han, K. Lead-Free Direct Band Gap Double-Perovskite Nanocrystals with Bright Dual-Color Emission. *J. Am. Chem. Soc.* **2018**, *140* (49), 17001–17006.

(8) Du, K.; Meng, W.; Wang, X.; Yan, Y.; Mitzi, D. B. Bandgap Engineering of Lead-Free Double Perovskite $Cs_2AgBiBr_6$ through Trivalent Metal Alloying. *Angew. Chem. Int. Ed.* **2017**, *56* (28), 8158–8162.

(9) Slavney, A. H.; Hu, T.; Lindenberg, A. M.; Karunadasa, H. I. A Bismuth-Halide Double Perovskite with Long Carrier Recombination Lifetime for Photovoltaic Applications. *J. Am. Chem. Soc.* **2016**, *138* (7), 2138–2141.

(10) McClure, E. T.; Ball, M. R.; Windl, W.; Woodward, P. M. Cs_2AgBiX_6 (X = Br, Cl): New Visible Light Absorbing, Lead-Free Halide Perovskite Semiconductors. *Chem. Mater.* **2016**, *28* (5), 1348–1354.

(11) Slavney, A. H.; Leppert, L.; Saldivar Valdes, A.; Bartesaghi, D.; Savenije, T. J.; Neaton, J. B.; Karunadasa, H. I. Small-Band-Gap Halide Double Perovskites. *Angew. Chem. Int. Ed.* **2018**, *57* (39), 12765–12770.

(12) Zhao, X.-G.; Yang, D.; Sun, Y.; Li, T.; Zhang, L.; Yu, L.; Zunger, A. Cu–In Halide Perovskite Solar Absorbers. *J. Am. Chem. Soc.* **2017**, *139* (19), 6718–6725.

(13) Steele, J. A.; Pan, W.; Martin, C.; Keshavarz, M.; Debroye, E.; Yuan, H.; Banerjee, S.; Fron, E.; Jonckheere, D.; Kim, C. W.; et al. Photophysical Pathways in Highly Sensitive $Cs_2AgBiBr_6$ Double-Perovskite Single-Crystal X-Ray Detectors. *Adv. Mater.* **2018**, *30* (46), 1804450.

(14) Pan, W.; Wu, H.; Luo, J.; Deng, Z.; Ge, C.; Chen, C.; Jiang, X.; Yin, W.-J.; Niu, G.; Zhu, L.; et al. $Cs_2AgBiBr_6$ Single-Crystal X-Ray Detectors with a Low Detection Limit. *Nature Photon.* **2017**, *11* (11), 726–732.

(15) Luo, J.; Wang, X.; Li, S.; Liu, J.; Guo, Y.; Niu, G.; Yao, L.; Fu, Y.; Gao, L.; Dong, Q.; et al. Efficient and Stable Emission of Warm-White Light from Lead-Free Halide Double Perovskites. *Nature* **2018**, *563* (7732), 541–545.

(16) Zhou, L.; Xu, Y.-F.; Chen, B.-X.; Kuang, D.-B.; Su, C.-Y. Synthesis and Photocatalytic Application of Stable Lead-Free $Cs_2AgBiBr_6$ Perovskite Nanocrystals. *Small* **2018**, *14* (11), 1703762.

(17) Greul, E.; Petrus, M. L.; Binek, A.; Docampo, P.; Bein, T. Highly Stable, Phase Pure $Cs_2AgBiBr_6$ Double Perovskite Thin Films for Optoelectronic Applications. *J. Mater. Chem. A* **2017**, *5* (37), 19972–19981.

(18) Pantaler, M.; Cho, K. T.; Queloz, V. I. E.; García Benito, I.; Fettkenhauer, C.; Anusca, I.; Nazeeruddin, M. K.; Lupascu, D. C.; Grancini, G. Hysteresis-Free Lead-Free Double-Perovskite Solar Cells by Interface Engineering. *ACS Energy Lett.* **2018**, *3* (8), 1781–1786.

(19) Ning, W.; Wang, F.; Wu, B.; Lu, J.; Yan, Z.; Liu, X.; Tao, Y.; Liu, J.-M.; Huang, W.; Fahlman, M.; et al. Long Electron–Hole Diffusion Length in High-Quality Lead-Free Double Perovskite Films. *Adv. Mater.* **2018**, *30* (20), 1706246.

(20) Sun, Q.; Wang, J.; Yin, W.-J.; Yan, Y. Bandgap Engineering of Stable Lead-Free Oxide Double Perovskites for Photovoltaics. *Adv. Mater.* **2018**, *30* (15), 1705901.

(21) Xiao, Z.; Du, K.-Z.; Meng, W.; Wang, J.; Mitzi, D. B.; Yan, Y. Intrinsic Instability of $Cs_2In(I)M(III)X_6$ (M = Bi, Sb; X = Halogen) Double Perovskites: A Combined Density Functional Theory and Experimental Study. *J. Am. Chem. Soc.* **2017**, *139* (17), 6054–6057.

(22) Majher, J. D.; Gray, M. B.; Strom, T. A.; Woodward, P. M. $Cs_2NaBiCl_6:Mn^{2+}$—A New Orange-Red Halide Double Perovskite Phosphor. *Chem. Mater.* **2019**, *31* (5), 1738–1744.

(23) K, N. N.; Nag, A. Synthesis and Luminescence of Mn-Doped $Cs_2AgInCl_6$ Double Perovskites. *Chem. Commun.* **2018**, *54* (41), 5205–5208.

(24) Fu, R.; Chen, Y.; Yong, X.; Ma, Z.; Wang, L.; Lv, P.; Lu, S.; Xiao, G.; Zou, B. Pressure-Induced Structural Transition and Band Gap Evolution of Double Perovskite $Cs_2AgBiBr_6$ Nanocrystals. *Nanoscale* **2019**, *11* (36), 17004–17009.

(25) Yang, E.; Luo, X. Theoretical Pressure-Tuning Bandgaps of Double Perovskites $A_2(BB')X_6$ for Photo-Voltaics. *Solar Energy* **2020**, *207*, 165–172.

(26) Lin, J.; Chen, H.; Gao, Y.; Cai, Y.; Jin, J.; Etman, A. S.; Kang, J.; Lei, T.; Lin, Z.; Folgueras, M. C.; et al. Pressure-Induced Semiconductor-to-Metal Phase Transition of a Charge-Ordered Indium Halide Perovskite. *Proc. Natl. Acad. Sci. U. S. A.* **2019**, *116* (47), 23404–23409.

(27) Li, Q.; Wang, Y.; Pan, W.; Yang, W.; Zou, B.; Tang, J.; Quan, Z. High-Pressure Band-Gap Engineering in Lead-Free $Cs_2AgBiBr_6$ Double Perovskite. *Angew. Chem. Int. Ed.* **2017**, *56* (50), 15969–15973.

(28) Zhang, L.; Liu, C.; Wang, L.; Liu, C.; Wang, K.; Zou, B. Pressure-Induced Emission Enhancement, Band-Gap Narrowing, and Metallization of Halide Perovskite $Cs_3Bi_2I_9$. *Angew. Chem.* **2018**, *130* (35), 11383–11387.

(29) Zhang, L.; Fang, Y.; Sui, L.; Yan, J.; Wang, K.; Yuan, K.; Mao, W. L.; Zou, B. Tuning Emission and Electron–Phonon Coupling in Lead-Free Halide Double Perovskite $Cs_2AgBiCl_6$ under Pressure. *ACS Energy Lett.* **2019**, *4* (12), 2975–2982.

(30) Jiang, J.; Niu, G.; Sui, L.; Wang, X.; Zhang, Y.; Che, L.; Wu, G.; Yuan, K.; Yang, X. Transformation between the Dark and Bright Self-Trapped Excitons in Lead-Free Double-Perovskite $Cs_2NaBiCl_6$ under Pressure. *J. Phys. Chem. Lett.* **2021**, *12* (30), 7285–7292.

(31) Kresse, G.; Furthmüller, J. Efficient Iterative Schemes for Ab Initio Total-Energy Calculations Using a Plane-Wave Basis Set. *Phys. Rev. B* **1996**, *54* (16), 11169–11186.

(32) Kresse, G. Ab Initio Molecular Dynamics for Liquid Metals. *J. Non-Cryst. Solids* **1995**, *192–193*, 222–229.

(33) Kresse, G.; Joubert, D. From Ultrasoft Pseudopotentials to the Projector Augmented-Wave Method. *Phys. Rev. B* **1999**, *59* (3), 1758–1775.

(34) Blöchl, P. E. Projector Augmented-Wave Method. *Phys. Rev. B* **1994**, *50* (24), 17953–17979.

(35) Perdew, J. P.; Burke, K.; Ernzerhof, M.

Generalized Gradient Approximation Made Simple. *Phys. Rev. Lett.* **1996**, *77* (18), 3865–3868.
(36) Heyd, J.; Scuseria, G. E.; Ernzerhof, M. Hybrid Functionals Based on a Screened Coulomb Potential. *J. Chem. Phys.* **2003**, *118* (18), 8207–8215.
(37) Paier, J.; Marsman, M.; Hummer, K.; Kresse, G.; Gerber, I. C.; Ángyán, J. G. Screened Hybrid Density Functionals Applied to Solids. *J. Chem. Phys.* **2006**, *124* (15), 154709.
(38) Albrecht, S.; Reining, L.; Del Sole, R.; Onida, G. Ab Initio Calculation of Excitonic Effects in the Optical Spectra of Semiconductors. *Phys. Rev. Lett.* **1998**, *80* (20), 4510–4513.
(39) Rohlfing, M.; Louie, S. G. Electron-Hole Excitations in Semiconductors and Insulators. *Phys. Rev. Lett.* **1998**, *81* (11), 2312–2315.
(40) Maintz, S.; Deringer, V. L.; Tchougréeff, A. L.; Dronskowski, R. LOBSTER: A Tool to Extract Chemical Bonding from Plane-Wave Based DFT. *J. Comput. Chem.* **2016**, *37* (11), 1030–1035.
(41) Maintz, S.; Deringer, V. L.; Tchougréeff, A. L.; Dronskowski, R. Analytic Projection from Plane-Wave and PAW Wavefunctions and Application to Chemical-Bonding Analysis in Solids. *J. Comput. Chem.* **2013**, *34* (29), 2557–2567.
(42) Smit, W. M. A.; Dirksen, G. J.; Stufkens, D. J. Infrared and Raman Spectra of the Elpasolites $Cs_2NaSbCl_6$ and $Cs_2NaBiCl_6$: Evidence for a Pseudo Jahn-Teller Distorted Ground State. *J. Phys. Chem. Solids* **1990**, *51* (2), 189–196.
(43) Zhao, X.-G.; Yang, J.-H.; Fu, Y.; Yang, D.; Xu, Q.; Yu, L.; Wei, S.-H.; Zhang, L. Design of Lead-Free Inorganic Halide Perovskites for Solar Cells via Cation-Transmutation. *J. Am. Chem. Soc.* **2017**, *139* (7), 2630–2638.